Journal of the Korean Society of Oceanography
Vol. 35, No. 2, pp. 65—77 June 2000

An Estimation of Tidal Currents from Satellite-tracked Drifters and its Application to the Yellow Sea

HEUNG-JAE LIE*, SEOK LEE, CHEOL-HO CHO AND SOK-KUH KANG[1]
Physical Oceanography Division, Korea Ocean Research and Development Institute,
[1]*Coastal and Harbor engineering Center, Korea Ocean Research and Development Institute,*
Ansan, P.O. Box 29, Seoul 425-600, Korea

A simple but effective method has been developed for estimating diurnal and semi-diurnal tidal currents from trajectories of satellite-tracked drifters. The estimation method consists of separation of tidal current signals contained in the drifter trajectories, computation of undulations by diurnal and semi-diurnal currents, and correction of dominant diurnal and semi-diurnal tidal constituents. M_2 tidal currents estimated from drifter trajectories in the Yellow Sea are well consistent with those observed by moored current meters and this supports the validity of this method. We have constructed M_2 tidal current chart in the Yellow Sea by applying this method to available drifter trajectories collected during 1994–1998. According to this chart, M_2 current in the Yellow Sea rotates in the clockwise direction south of 35° 30'N but in the counterclockwise one to the north. Also it is found that the M_2 current is strong in the bank area northeast of the Changjiang River mouth and in the Korean coastal area, while it is weak in the deep central trough.

INTRODUCTION

Tides in the Yellow Sea are one of key factors controlling oceanographic structures and marine environments of the Yellow Sea (YS). Strong tidal current regime of the YS are engaged in major coastal oceanographic processes such as formation of tidal fronts, transport of sea waters and materials, and mixing.

Numerical tide models for the YS (An, 1977; Choi, 1980; Guo and Yanagi, 1998; Kang *et al.*, 1991, 1998) can reproduce coastal sea level changes with high accuracy and satisfactorily explain the observed tidal regime of complex amphidromies (Ogura, 1933; Nishida, 1980). Sea levels in the YS have been monitored for long periods at a series of coastal tidal stations along the Korean and Chinese coast. However, offshore sea levels and tidal currents have not been well described mainly due to insufficient observations in the offshore area. Although numerical tidal models provide information on the tidal current system, model currents are very dependent upon various model parameters such as grid spacing, bottom topography, and viscosity including bottom drag coefficient. Shoaling bottom topography, rugged coastline, and a lot of small islands and tidal channels in the YS cannot be well resolved in the basin-scale models with grid spacing of 5 to 10 km. Therefore, the model currents are needed to be compared with observed currents to assess how accurately tidal currents are reproduced.

The Korea Ocean Research and Development Institute (KORDI) deployed a relatively large number of satellite-tracked drifters at many places during 1994–1998. The drifters are limited to measure currents at predetermined drogue depths and satellite passages, but they are cost-effective and have an advantage to provide current information over a large area. Drifter trajectories contain current signals in frequency bands lower than the cut-off frequency defined by $1/(2\Delta t)$, where Δt is time interval between two consecutive position fixes sensed at the ARGOS system. In the YS, the mean time interval is about 4 hours, so current signals having periods longer than 8 hours are resolved. Therefore, dominant semi-diurnal and diurnal tidal currents in the YS can be estimated by analyzing drifter trajectories. In this study we first introduce a new, simple method of separating diurnal and semi-diurnal currents in the drifter trajectories, computing semi-diurnal and diurnal tidal currents, and correcting two major tidal currents M_2 and K_1 using

*Corresponding author: hjlie@kordi.re.kr

undulations. Next, the validity of the estimation is examined by applying this method to both sea levels and tidal currents observed in the YS. Finally, we have attempted to construct M_2 tidal current chart of the YS from all available drifter trajectories in the YS.

DRIFTER DATA

The KORDI deployed ARGOS drifters in the YS and East China Sea at thirteen times during 1994-1998 to collect current data for the basin-scale shelf circulation (Lie, 1998a; 1998b). For this study, we have used 73 drifter trajectories that were observed longer than five days and wandered in the YS and the YS-East China Sea boundary. Of the 73 drifters, 64 sets had a holey-sock drogue of WOCE prototype (Sybrandy and Niiler, 1987) and other 9 sets had a cross window-shaped drogue centered at 0.5 m. The holey-sock drogues were centered at a depth of 15 m below sea surface (50 sets) and at depths of 30 m or deeper (14 sets).

All drifters were set to transmit signals continuously for the first 30 days after release and then during 8 hours a day for the remaining lifetime. In case of the continuous transmission, drifter positions are sensed at 2 to 5 hours intervals around Korea, with a mean sensing frequency of about 6.1 times per day. We used only the continuous position fixes for a better estimation of tidal currents. Fig. 1 shows a composite map of all 73 drifter trajectories. Cross marks indicate release points of drifters. Table 1 summarizes number of drifters and mean lifetime in warm and cold seasons. The mean lifetime in the warm season (May to October) is almost twice longer than that in the cold season (November to April). The shorter lifetime in the cold season is mainly due to strong fishing activity in the cold season in the YS.

Table 1. General information of drifter experiments performed in the Yellow Sea during 1994 to 1998

Periods	Number of drifters	Mean lifetime (day)	Data length sensed continuously relative to the total length (day)
May to Oct.	36	52.0	1096/1872
Nov. to Apr.	37	26.3	736/972

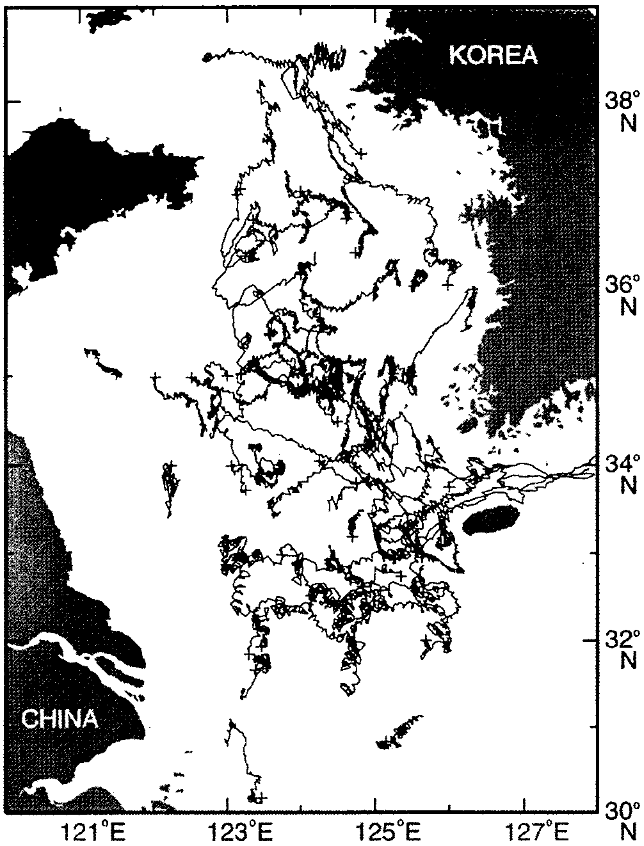

Fig. 1. Trajectories of satellite-tracked drifters deployed by KORDI in the Yellow Sea during 1994–1998. Symbols + indicate release points of drifters.

SEPARATION OF HIGH- AND LOW-FREQUENCY CURRENTS

Drifter trajectories, $X_d(r, t)$, at position r and time t are decomposed into three parts as follows:

$$X_d(r, t) = X_0(r, t) + X(r, t) + Er(t) \quad (1)$$

where $X_0(r, t)$ is position determined by low-frequency currents, $X(r, t)$ is position by high-frequency currents, and Er is positioning errors.

Drifter positions are determined at time intervals of 2–5 hours between two successive satellite passes, with position errors of 150–350 m. Since velocities are estimated from position displacements during individual time intervals, velocity errors do not exceed 5 cm/s. This errors are small as compared to observed currents of 10–100 cm/s in the YS. Slippage due to wind is below 2 cm/s in winds of 20 m/s (WOCE, 1991), so it is negligibly small as compared to other error sources.

Low-frequency currents

In general, low-frequency currents in the YS are not so strong as high-frequency tidal currents in the interior YS (Lie, 1999), although relatively strong currents are intermittently generated during the winter monsoon (Hsueh, 1988) and mean currents, comparable to tidal currents, exist around Cheju-do (Lie *et al.*, 2000). Since scales of the low-frequency currents are larger in space and longer in time than those of the tidal currents, drifter displacement by the low-frequency currents can be fitted to summation of polynomials within a short time span of T or estimated by using a low-pass filter. In this study, the drifter displacements are simply least-squared fitted to the second-order polynomials as below.

$$X_o(r,t) \approx a_0 + a_1 t + a_2 t^2 \quad \text{for} \quad -T/2 \le t \le T/2 \tag{2}$$

where a_0, a_1 and a_2 are arbitrary constants.

High-frequency tidal currents

Drifter displacements by the high-frequency tidal currents can be approximated to sum of a series of displacements by major tidal current constituents.

$$X(r,t) \approx \sum_{i=1}^{N} X_i(r,t) \tag{3}$$

$$X_i(r,t) = A_i(r)\cos(\omega_i t - \theta_i(r)) \quad \text{for} \quad -T/2 \le t \le T/2 \tag{4}$$

where N is number of tidal constituents to be considered, ω_i frequency of ith constituent, $A_i(r)$ and θ_i (r) amplitude and phase. $A_i(r)$ and $\theta_i(r)$ are space-dependant variables. The tidal displacements during T are within the corresponding tidal excursions in an area where the low-frequency currents are relatively very weak, so that the amplitude and phase are assumed to be space-independent variables over the displacements. This assumption can be applied to strong low-frequency current area if shorter T is properly chosen.

$$X_i(r,t) \approx X_i(t) = A_i\cos(\omega_i t - \theta_i) \quad \text{for} \quad -T/2 \le t \le T/2 \tag{5}$$

Tidal currents are given by

$$\boldsymbol{U}_i(t) = \frac{dX_i}{dt} = A_i\omega_i\cos(\omega_i t + \pi/2 - \theta_i) \quad \text{for} \quad -T/2 \le t \le -T/2 \tag{6}$$

Relation between time interval and resolution of tidal harmonics

The time interval T of boxcar window should be carefully determined by considering sampling intervals of drifter position data, resolution of tidal harmonics, and space-dependency of tide harmonic constants. According to the Rayleigh criteria $|\Delta f|T>1$, where Δf is frequency difference between two harmonics, the two harmonics can be separated in a time series data of which the observation duration is longer than synodic period of the two harmonics. For given frequencies of the two harmonics, the harmonics can be separated using only four data points, but background noises in the observed data make the separation difficult. Munk *et al.* (1964) suggested another criteria $|\Delta f|T>s^{1/2}$, where s is the signal-to-noise level. For small s, two harmonics are separated from a time series shorter than the synodic period of the harmonics.

For longer T, more constituents can be separated, but the space-independence of tidal constituents in equation (4) may not be maintained. On the other hand, shorter T can be applied to strong low-frequency current area, but the frequency resolution becomes worse. To choose proper T for estimating M_2 currents in the YS, three cases T equal to 4, 5, and 6 days were tested. Although the results are not significantly different, we have fixed T=5 day for this study because M_2 in the southeastern YS is estimated with a little higher accuracy.

ESTIMATION OF DIURNAL AND SEMI-DIURNAL TIDAL CURRENTS

In the YS, the diurnal and semi-diurnal currents are much more dominant than the low-frequency residual currents. The time span of 5 days is not long enough to separate the major 5 tidal constituents, M_2, S_2, N_2, K_1 and O_1 (e.g., Choi, 1980). Therefore, as the first step of analysis, we approximate tidal currents $\boldsymbol{U}_i(t)$ to sum of diurnal and semi-diurnal currents of which frequencies are centered at M_2 and K_1 frequencies.

$$\boldsymbol{U}_i(t) \approx \boldsymbol{U}_s(t) + \boldsymbol{U}_d(t) \quad \text{for} \quad -T/2 \le t \le T/2 \tag{7a}$$

$$\boldsymbol{U}_s = U_s\,\boldsymbol{i} + V_s\boldsymbol{j} \tag{7b}$$

$$\boldsymbol{U}_d = U_d\boldsymbol{i} + V_d\boldsymbol{j} \tag{7c}$$

where $\boldsymbol{U}_s$ and $\boldsymbol{U}_d$ are semi-diurnal and diurnal tidal currents, $\boldsymbol{i}$ and $\boldsymbol{j}$ are the east and north unit vectors in the ordinary x-y coordinates, U_s and U_d the east components of diurnal and semi-diurnal currents, and V_s and V_d the corresponding north components.

To estimate major tidal currents from truncated drifter data having T=5 days, we have developed a new technique that uses undulation of two tidal constituents and corrects a specific constituent for contribution of other constituents to the specific constituent. The correction method is similar to that of Zetler *et al.* (1965) who have corrected K_1 for the contribution of P_1, S_2 for K_2 and T_2, and N_2 for ν_2,

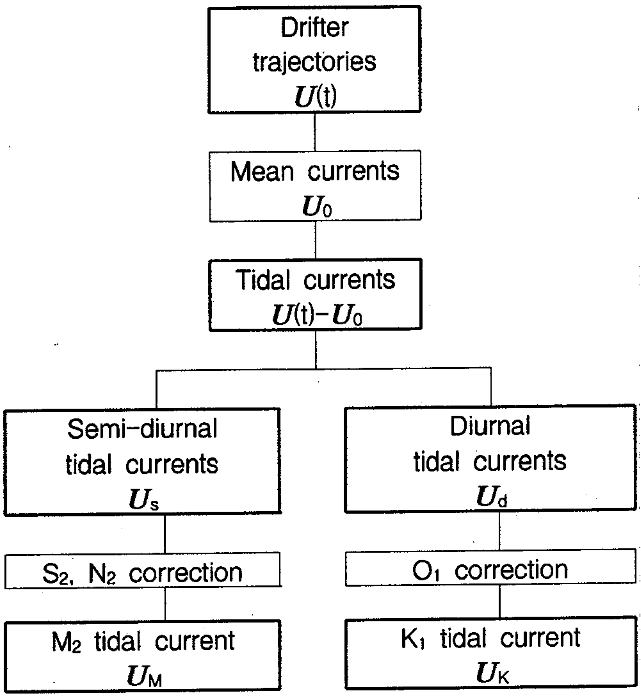

Fig. 2. Flow chart for estimating tidal currents from drifter trajectories.

using amplitude ratios and phase relationships. Flow chart in Fig. 2 shows the computing procedure of semi-diurnal and diurnal tidal currents from the drifter trajectories.

Semi-diurnal currents

The east semi-diurnal tidal currents in (7b) can be expressed by a single harmonic function within a boxcar window.

$$U_s(t) = A\cos\{\omega t + v_M(t_0) - \theta\} \quad (8a)$$
$$= A_C\cos\phi(t) + A_S\sin\phi(t) \quad (8b)$$

where t_0 is reference time, ω is angular velocity of M_2, A, θ are amplitude and phase, $v_M(t_0)$ is equilibrium phase of M_2 at t_0, A_C=A cos θ, A_S=A sin θ, $\phi(t)=\omega t+v_M(t_0)$. $U_s(t)$ composes mainly of three major semi-diurnal currents of M_2, S_2, and N_2.

Equation (8a) is approximated as follows:

$$U_S(t) = U_M(t) + U_S(t) + U_N(t) \quad (9a)$$
$$U_M(t) = f_M(t)M\cos\{\phi(t) + u_M(t) - \theta_M\} \quad (9b)$$
$$U_S(t) = g_s S\cos\{\phi(t) - v_M(t_0) + v_S(t_0) + \Delta_1 t - \theta_S\} \quad (9c)$$
$$U_N(t) = f_N(t)g_n N\cos\{\phi(t) - v_M(t_0) + v_N(t_0) + u_N(t) + \Delta_2 t - \theta_N\} \quad (9d)$$

where M, S, N are amplitudes of M_2, S_2 and N_2,
θ_M, θ_S, θ_N are phases of M_2, S_2 and N_2,
f_M, f_N, u_M, u_N are nodal factors,
$v_S(t_0)$, $v_N(t_0)$ are equilibrium phases of S_2 and N_2 at t_0,
$\Delta_1=\omega_S-\omega$, $\Delta_2=\omega_N-\omega$ are angular velocity differences between S_2 and M_2, and between N_2 and M_2,
ω_S, ω_N are angular velocities of S_2 and N_2,
g_s, g_n are contribution rates of S_2 and N_2 to M_2.

We introduce amplitude ratios (C_S, C_N), phase differences (φ_S, φ_N), contribution rates of S_2 and N_2 to M_2, defined as follows:

$$C_S = \frac{S}{M}, \quad \varphi_S = \theta_M - \theta_S \quad (10a)$$
$$C_N = \frac{N}{M}, \quad \varphi_N = \theta_M - \theta_N \quad (10b)$$
$$g_s = \frac{\sin\left(\frac{T}{2}\Delta_1\right)}{\frac{T}{2}\Delta_1}, \quad g_n = \frac{\sin\left(\frac{T}{2}\Delta_2\right)}{\frac{T}{2}\Delta_2} \quad (10c)$$

These six coefficients in (10) are defined as 'correction coefficients' for M_2 current. g_s and g_n vary with time span T. By replacing unknown amplitudes and phases of S_2 and N_2 in (9) by the correction coefficients, (9) is rearranged as follows:

$$U_M(t) = F_M M\cos\{\phi(t) + \Phi_M(t_0) - \theta_M\} \quad (11a)$$
$$U_S(t) = F_S M\cos\{\phi(t) + \Phi_S(t_0) - \theta_M\} \quad (11b)$$
$$U_N(t) = F_N M\cos\{\phi(t) + \Phi_N(t_0) - \theta_M\} \quad (11c)$$

where $F_M=f_M$, $F_S=C_S g_s$, $F_N=f_N C_N g_n$, $\Phi_M=u_M(t)$,
$\Phi_S=-v_M(t_0)+v_S(t_0)+\varphi_S$, $\Phi_N=-v_M(t_0)+v_N(t_0)+u_N(t)+\varphi_N$.

The amplitude and phase of M_2 can be calculated as follows:

$$M = \sqrt{\frac{A_C^2+A_S^2}{FC^2+FS^2}} \quad (12a)$$
$$\theta_M = \tan^{-1}\left[\frac{A_C FS + A_S FC}{A_C FC - A_S FS}\right] \quad (12b)$$

where $FC = F_M\cos\Phi_M + F_S\cos\Phi_S + F_N\cos\Phi_N$
$FS = F_M\sin\Phi_M + F_S\sin\Phi_S + F_N\sin\Phi_N$

The northward M_2 current can be calculated in the same way.

Diurnal currents

The diurnal tidal currents also can be obtained similarly. The east diurnal currents are expressed as follows;

$$U_d(t) = B(t)\cos\{\omega_K t + v_K(t_0) - \theta(t)\} \quad (13a)$$

$$U_d(t) = B_C\cos\phi(t) + B_S\sin\phi(t) \qquad (13b)$$

where B, θ are amplitude and phase of diurnal component, ω_K is angular velocity of K_1, $v_K(t_0)$ is equilibrium phase of K_1 at the reference time t_0, $B_C = B\cos\theta$, $B_S = B\sin\theta$, $\phi(t) = \omega_K t + v_K(t_0)$.

The diurnal tidal currents compose mainly of two major constituents of O_1 and K_1.

$$U_d(t) = U_K(t) + U_O(t) \qquad (14a)$$

$$U_K(t) = f_K(t) K\cos\{\phi(t) + u_K(t) - \theta_K\} \qquad (14b)$$

$$U_O(t) = f_O(t) g_o O\cos\{\phi(t) - v_K(t_0) + v_O(t_0) + u_O(t) + \Delta_3 t - \theta_O\} \qquad (14c)$$

where K, O are amplitude of K_1 and O_1,
θ_K, θ_O are phase of K_1 and O_1,
f_K, f_O, u_K, u_O are nodal factors,
$v_O(t_0)$ is equilibrium phase of O_1 at to,
$\Delta_3 = \omega_O - \omega_K$ is difference of angular velocity between O_1 and K_1,
ω_O is angular velocity of O_1,
g_o is contribution rate of O_1 to K_1.

The correction coefficients for K_1 current are defined as follows:

$$C_O = \frac{O}{K},\ \varphi_O = \theta_K - \theta_O,\ g_o = \frac{\sin\left(\frac{T}{2}\Delta_3\right)}{\frac{T}{2}\Delta_3} \qquad (15)$$

The amplitude and phase of K_1 are given as follows:

$$K = \sqrt{\frac{B_C^2 + B_S^2}{GC^2 + GS^2}} \qquad (16a)$$

$$\theta_K = \tan^{-1}\left[\frac{B_C GS + B_S GC}{B_C GC - B_S GS}\right] \qquad (16b)$$

where $GC = f_K\cos u_K + \frac{f_O C_O}{g_o}\cos(-v_K + v_O + u_O + \varphi_O)$

$$GS = f_K\sin u_K + \frac{f_O C_O}{g_o}\sin(-v_K + v_O + u_O + \varphi_O)$$

VALIDITY TESTS OF THE ESTIMATION METHOD

In order to check the validity of the estimation method developed in former section, two tests were preformed by applying this method to both sea levels generated by five major tidal constituents and current data observed at 11 mooring points in the YS (Fig. 3). The time span T is set to five days. Low-frequency residual signals in the truncated data are estimated by the second-order polynomial fitting method.

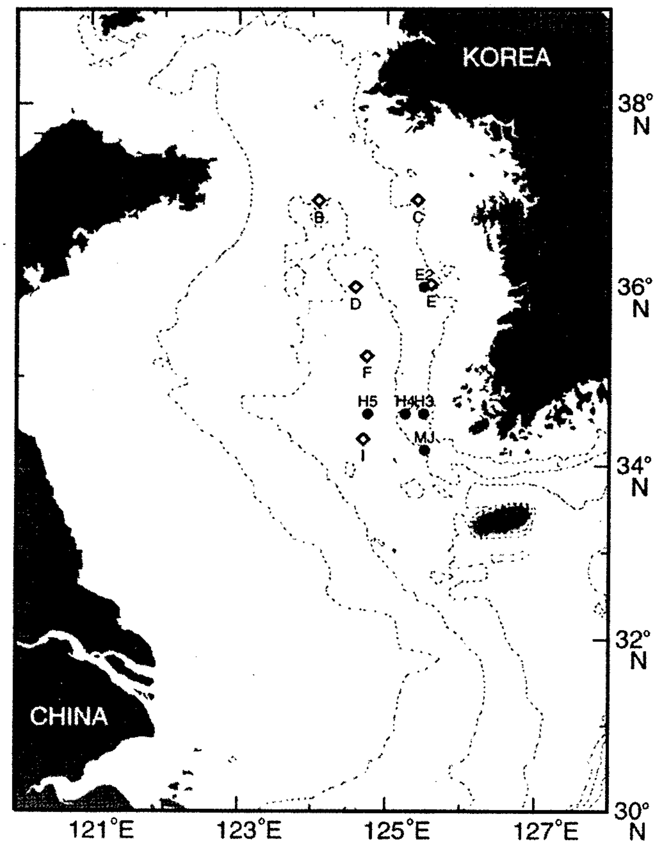

Fig. 3. Bottom topography in meters and location of current meter moorings in the Yellow Sea. Symbols of open diamond and dark circle denote respectively moorings of Florida State University(◇) (Hsueh, 1988) and KORDI(●) (Lie, 1998b).

Test 1: model tide

Time sequential sea levels were generated at randomly selected 180 points in the YS between 122°E –126°E, and 32°N–38°N, using harmonic constants of five major tidal constituents (M_2, S_2, N_2, K_1, O_1) computed by a two-dimensional tide model of Kang *et al.* (1998). The model results are in good agreement with observed tides and tidal currents in the offshore area of YS. The generated time series were re-sampled at the similar sampling intervals of drifter data. By applying our new method to the 180 time series, we have estimated semi-diurnal and M_2 tides and then compared the estimated values with the model harmonic constants of M_2 used for the data generation.

Fig. 4 shows comparisons of the estimated semi-diurnal and M_2 tides with the model M_2 tides. Amplitudes and phases of the estimated semi-diurnal tides have large variations around the model M_2 tides (Fig. 4a). The variation ranges of amplitudes and phases

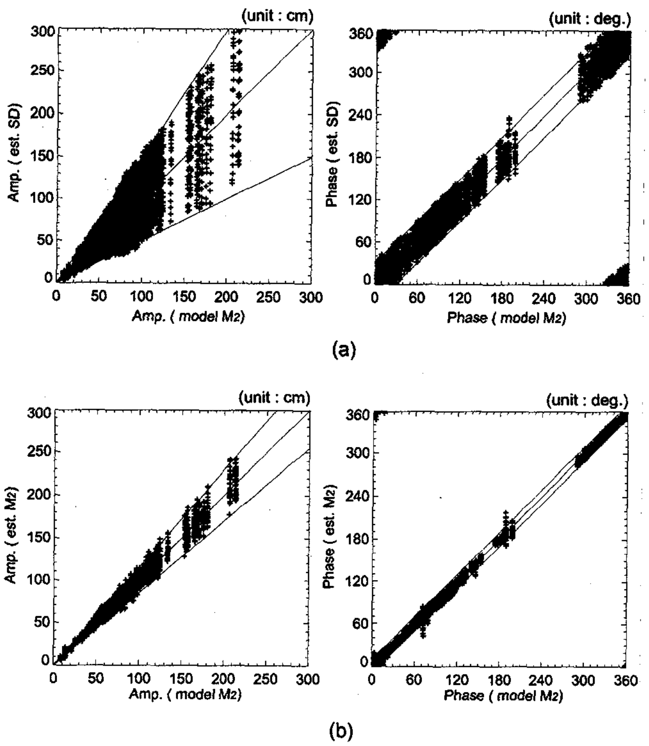

Fig. 4. Comparisons between model M_2 tides and estimated semi-diurnal and M_2 tides. Time sequential sea level data of which the length is 5 days are generated by five major harmonic constants of M_2, S_2, N_2, K_1, and O_1. (a) estimated semi-diurnal tide versus model M_2 tide and (b) estimated M_2 tide versus model M_2 tide.

are about ±50% of the model M_2 amplitudes and ±30 degrees of the model M_2 phases, respectively. The phase range of 30 degrees corresponds to about one hour difference in phase. These discrepancies between estimated semi-diurnal and model M_2 tides are mainly due to the undulation with synodic periods of M_2 and S_2 and/or N_2, and partly due to the data truncation. Table 2 shows mean correction coefficients of amplitude ratios and phase difference at the 180 points. Sum of the mean amplitude ratios of C_S and C_N is 0.56, which accounts well for the variation ranges of amplitude of ±50% and of phase of ±26 degrees in Fig. 4a.

Estimated M_2 tides, corrected for the contribution of S_2 and N_2, are compared with the model M_2 tides (Fig. 4b). The variation ranges are much reduced by the correction. The estimated M_2 tides are in good agreement with the model M_2 tides, within error ranges of ±15% for amplitude and ±10 degrees for phase. Since these error ranges result mainly from the data truncation, the error ranges may be diminished when T is longer than 5 days. Fig. 5 present comparison results for T=10 days. The error ranges

Table 2. Means and standard deviations of the correction coefficients of amplitude ratio and phase difference for M_2 tide in the Yellow Sea which are computed from 180 sea level time series

Correction coefficients	C_S	C_N	φ_S	φ_N
Mean	0.39	0.17	-38.0	27.9
Standard deviation	0.03	0.02	5.5	7.7

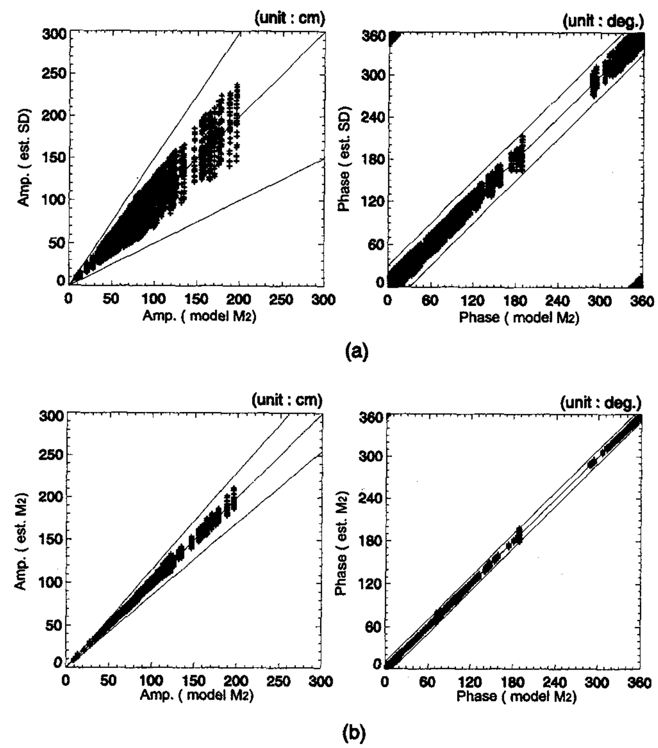

Fig. 5. Same as for Fig. 4, except longer data length of 10 days.

are reduced to almost half of those for T=5 days. For the practical purpose, the spatially averaged correction coefficients as in Table 2 may be used as the reference values, with exceptions near amphidromic points, unless reliable correction coefficients are provided.

Test 2: moored current data

Current measurements at 11 mooring points in Fig. 3 were conducted for about one month or longer. Progressive vector diagrams of these current data are considered as Lagrangian trajectories for test 2. The imaginary trajectories are re-sampled at the similar sampling intervals of observed trajectories and are truncated into time series of 5 days. The re-sampled times series have not position errors unlike the observed trajectories since they are originally from

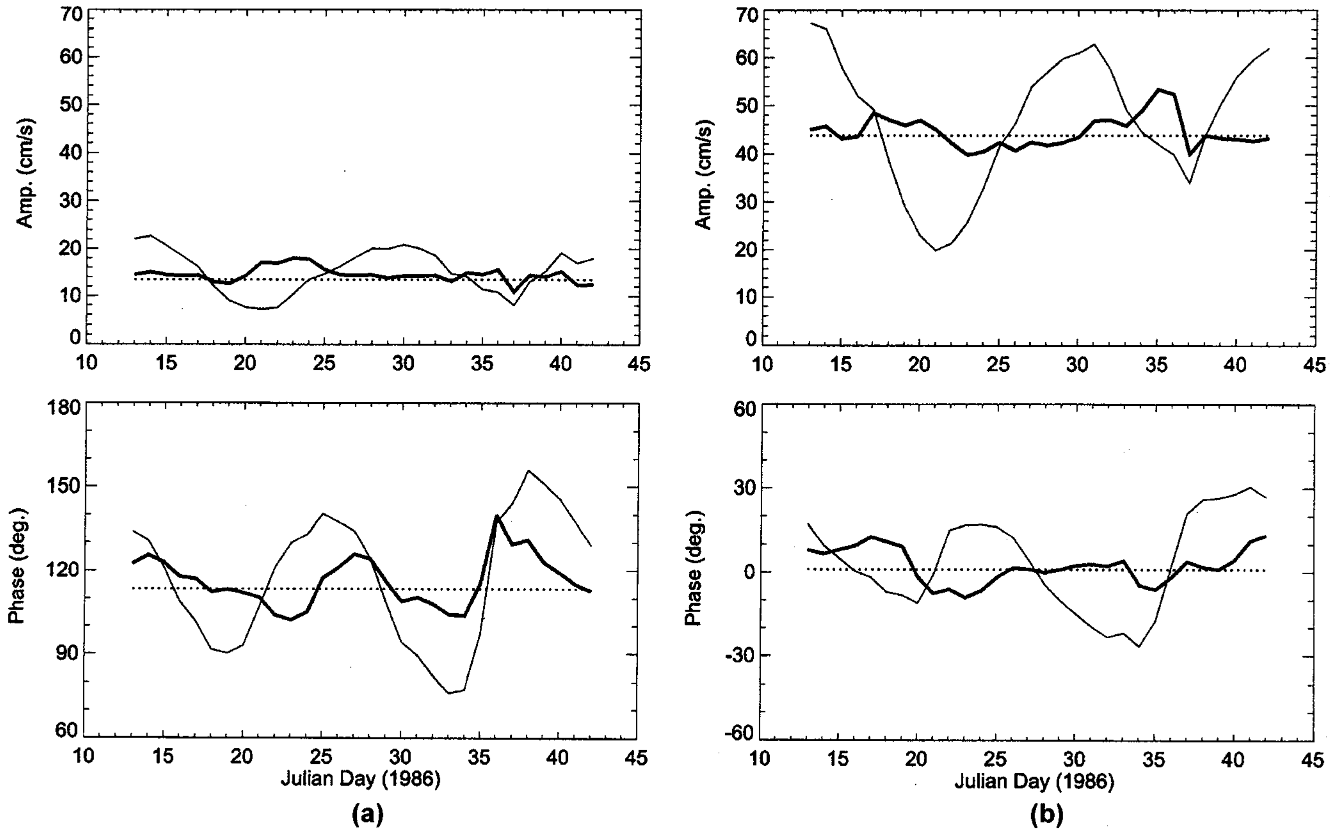

Fig. 6. Amplitudes and phases of estimated semi-diurnal (thin lines) and M_2 (thick lines) current components at mooring I in Fig. 3. (a) east current component and (b) north current component. Dashed line denotes amplitudes and phases of M_2 tidal currents from all moored data.

moored current data. Low-frequency residual currents are estimated using the second-order polynomial fitting and high-frequency tidal currents are obtained by subtracting the low-frequency currents from the re-sampled time series.

Fig. 6 shows amplitudes and phases of estimated semi-diurnal (thin lines) and M_2 (thick lines) currents at mooring I in the southern YS trough. Dashed lines correspond to amplitudes and phases of M_2 current which are computed by applying a tide harmonic analysis to the full current data observed during 33 days. For convenience, the amplitudes and phases from the full current data are named 'observed values' of M_2 current. Amplitudes and phases of the estimated semi-diurnal currents fluctuate around the observed values with an undulation having a period of about 15 days. The undulation period corresponds to the synodic period of M_2 and S_2. The undulation ranges are about 60–70% of the observed M_2 amplitude and 30–45 of the observed M_2 phase. After correction for the contribution by S_2 and N_2, the undulation ranges of estimated M_2 current are reduced to about half of the semi-diurnal ranges. Table 3 presents mean values of the correction coefficients for this test, computed from current data observed at 11 moorings in Fig. 3.

We also estimated amplitudes and phases of diurnal currents at mooring I (Fig. 7). The diurnal currents undulate with the K_1-O_1 synodic period of about 14 days. The undulations fluctuate more largely in time

Table 3. Means and standard deviations of the correction coefficients of amplitude ratio and phase difference for M_2 tidal current in the Yellow Sea which are computed from observed current data at 11 moorings marked Fig. 3

	U-comp.						V-comp.					
	C_S	C_N	C_O	φ_S	φ_N	φ_O	C_S	C_N	C_O	φ_S	φ_N	φ_O
Average	0.50	0.15	0.80	-77.6	27.0	64.6	0.45	0.17	0.70	-67.2	23.9	55.5
Standard deviation	0.04	0.02	0.12	9.7	12.5	11.6	0.04	0.01	0.05	4.6	4.5	7.1

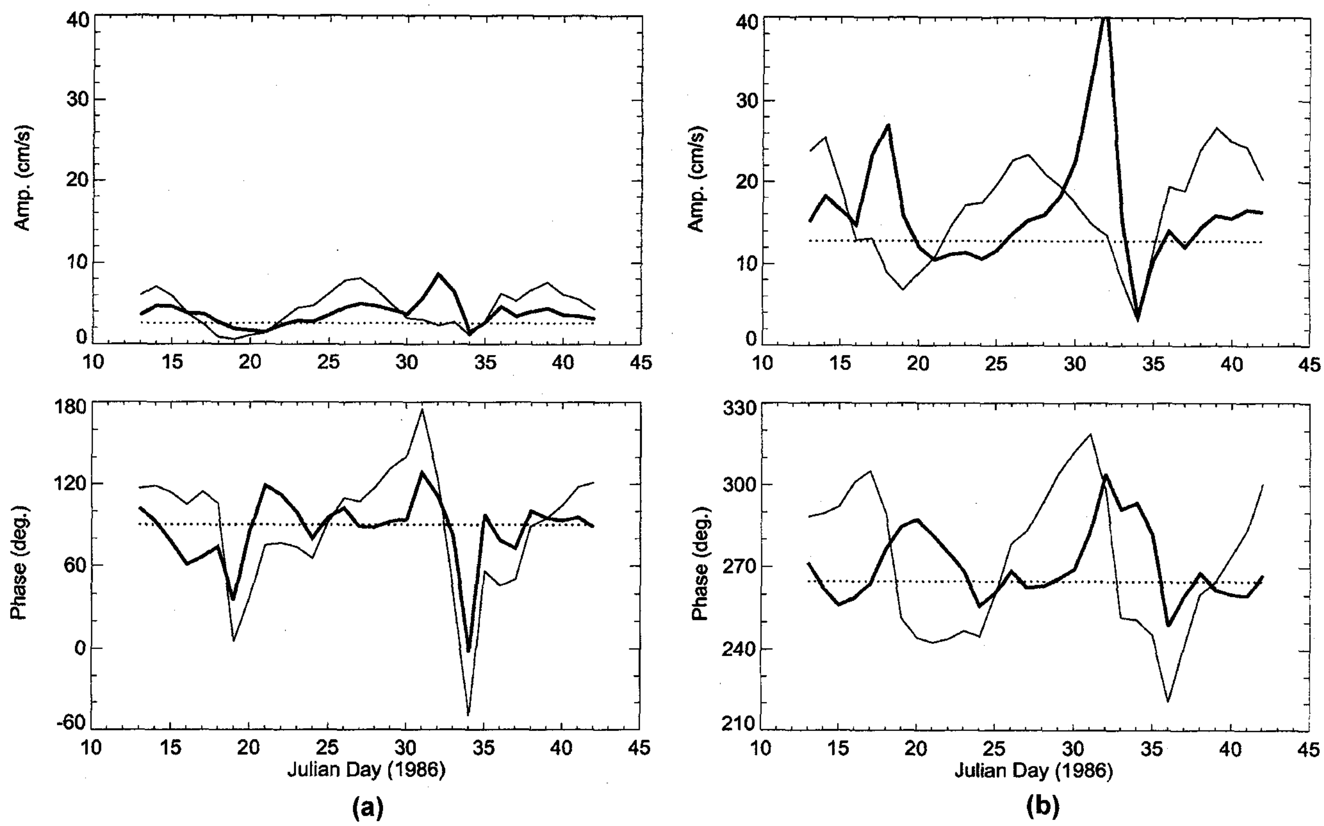

Fig. 7. Amplitudes and phases of estimated diurnal (thin lines) and K_1 (thick lines) current components at mooring I in Fig. 3. (a) east current component and (b) north current component. Dashed lines denote amplitudes and phases of K_1 tidal currents from all moored data.

as compared with those of semi-diurnal currents in Fig. 6. Magnitude of the amplitude undulation is greater than the observed K_1 amplitude. This large undulation is not reduced by correction for the contribution of O_1. Rather, the undulation of the K_1 north current increases. The large estimation error in the diurnal band may be caused by relatively high background noise level. At the mooring point I, the amplitude of K_1 current is about one thirds of M_2 current. If the background noise were assumed to be equally distributed in the semi-diurnal and diurnal frequency bands, the signal-to-noise level in the diurnal band would be three times larger than that in the semi-diurnal band.

Through the above two tests, it is found that this method is valid only for cases where the signal-to-noise levels are sufficiently small in frequency bands under consideration. At the current moorings in Fig. 3, root mean square values of low-frequency currents are below 5 cm/s. Because of relatively low signal-to-noise level in semi-diurnal frequency band, strong M_2 currents are effectively estimated with high accuracy by taking T=5 days. However, this time span is not proper for estimation of weaker diurnal currents in the YS since the signal-to-noise level remains high. To reduce the signal-to-noise level in the diurnal frequency band, a longer time span should be chosen, provided that low-frequency currents are very weak as compared with the diurnal tidal currents.

M_2 TIDAL CURRENTS IN THE YELLOW SEA

We compute M_2 tidal currents in the YS by applying the developed method to all available trajectories in Fig. 1. The drifter position data are truncated into pieces of five days (T=5 days). Fig. 8 shows computation locations of M_2 tidal currents which correspond to position of each truncated piece at the mid time of the five day duration. Diamonds denote locations of eleven current meter moorings and ellipses mark circular range of 0.2 degrees from the mooring points. Mean values of the correction coefficients for M_2 current in Table 3 are used for the computation.

As the first step, we compare M_2 tidal currents at two moorings with semi-diurnal and M_2 tidal currents

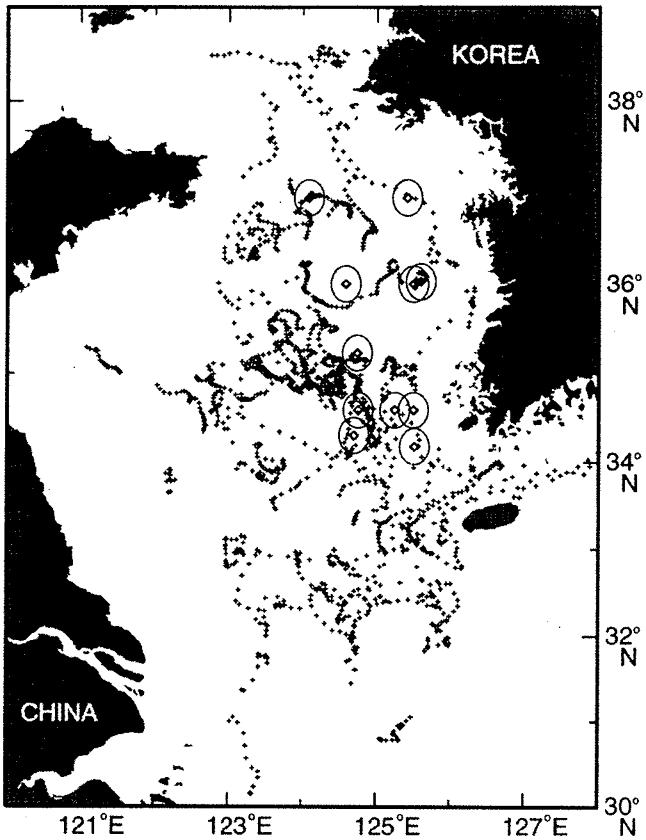

Fig. 8. Estimation points of tidal currents from drifter trajectories marked by + symbol. The diamond marks indicate current meter moorings and ellipses around the moorings correspond to a spatial distance of 0.2 degrees from the moorings.

computed from drifter data within the range of 0.2 degrees around the corresponding moorings. Fig. 9 is scatter plots of semi-diurnal (upper panel) and M_2 (lower panel) currents computed from drifter trajectories around mooring F (+symbols). The trajectories were those traced by a drifter having a drogue at 40 m. Thin arrows and circles indicate mean and root mean square (rms) currents. For a convenience of presentation, amplitude of each current component (U, V) is multiplied by cosine and sine functions of its corresponding phase (Pu, Pv) since each component is expressed by amplitude and phase. Therefore, the length of each arrow corresponds to amplitude and the angle of arrow from the x-axis counted in the counterclockwise direction corresponds to phase. On the other hand, thick arrows indicate M_2 currents at two depths of 70 and 95 m of mooring station F, which are computed using an ordinary tidal harmonic analysis. The observation length of moored current data are 39 days long and the water depth is 96 m. Semi-diurnal currents computed both from the drifter and moored current data show that the north component is much stronger than the east component. M_2 current at 70 m depth is much stronger than that at 95 m depth near the bottom. Although the observation time and depths are different, M_2 currents from the drifter data (Fig. 9d) are fairly consistent with that observed at 70 m depth within 10% for amplitude and about 10 degrees for phase. It is also seen that rms currents of the drifter data are much reduced by correcting M_2 current for S_2 and N_2.

Fig. 10 presents scatter plots of semi-diurnal and M_2 currents from trajectories around moorings E and E2 off the mid-west coast of Korea, and moored current data at three different depths. Amplitudes of the moored currents decrease with increasing depth. On the other hand, the mean currents computed from the drifter data have larger amplitudes and phases than the moored currents have. M_2 current vectors of the moored current data are not inside the rms current range. Large discrepancy in phase may result from various causes such as complicated bottom topography around the mooring points and different observation time and depths. The bottom topography around the moorings is shoaling and sloping. Averaging currents computed from truncated drifter data around the moorings smoothes out local change in tidal current induced by bottom topography. Drifters had drogue at 15 m and their positions were measured in spring during April 11 to May 11, 1996 when stratification was just established with thermocline near 20 m. On the other hand, the moored current data were collected in winter from January 11 to April 12, 1986 at the point E and from March 3 to April 4, 1984 at the point E2 when the water column was vertically homogeneous. The north component of mean M_2 current has larger amplitude by about 10% and phase difference of 17 degrees as compared to the moored current at 20 m depth. Such discrepancies are also detected when barotropic model currents are compared with moored currents in the deep central YS (Kang *et al.*, 1998). Therefore, the bottom topography is thought to be most responsible for the large discrepancies.

Semi-diurnal currents and M_2 currents computed from drifter trajectories around all moorings are compared with M_2 currents computed from the moored current data (Table 4). At each mooring, M_2 current at shallow depth is stronger that that at deeper depth and the mean M_2 current of the drifter data is closer to the moored M_2 current at the shallow depth.

Since the mean M_2 currents computed from drifter

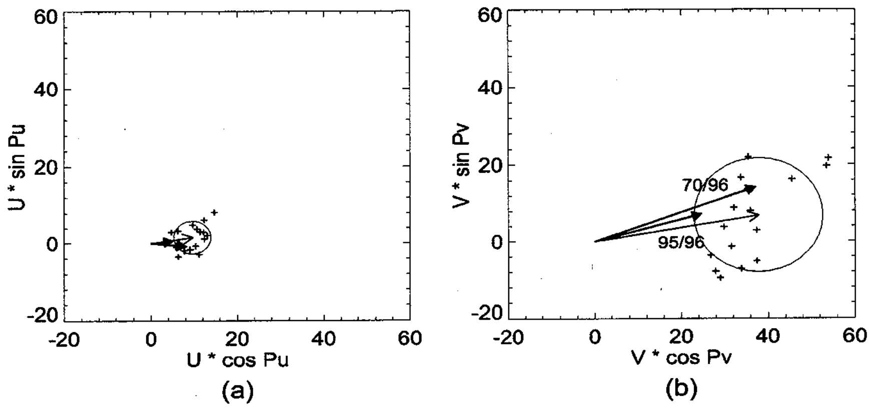

Fig. 9. Scatter plots of semi-diurnal and M_2 currents estimated from drifter trajectories within a 0.2 degree range from mooring F. (a) east semi-diurnal current, (b) north semidiurnal current, (c) east M_2 current and (d) north M_2 current. Thin arrows indicate mean vectors of estimated currents and circles correspond to rms ranges of the mean vectors. Thick arrow vectors indicate semi-diurnal and M_2 currents at mooring F. Numbers on thick arrows denote depths of current meters/water depth.

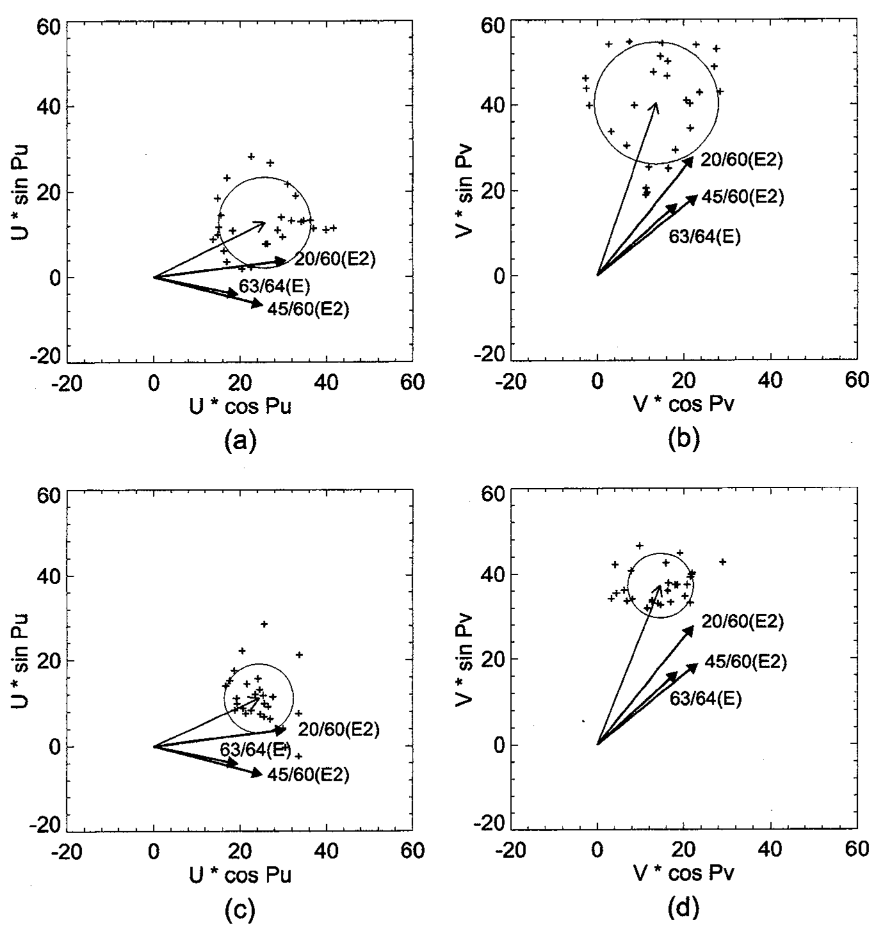

Fig. 10. Scatter plots of semidiurnal and M_2 currents estimated from drifter trajectories within a 0.2 degree range from mooring E and E2. Others are same as for Fig. 9.

Table 4. M_2 tidal currents computed from moored current data and semi-diurnal and M_2 tidal currents computed from satellite-tracked drifter trajectories in the Yellow Sea. Locations of current moorings are marked in Fig. 2.

Station	Meter depth /water depth	Period (mon/day /year)	Moored current data				No. of drifter	Drifter data							
			U-comp.		V-comp.			Semi-diurnal current data				M_2 current data			
								U-comp.		V-comp.		U-comp.		V-comp.	
			Amp. (cm/s)	Pha. (deg.)	Amp. (cm/s)	Pha. (deg.)		Amp.	Pha.	Amp.	Pha.	Amp.	Pha.	Amp.	Pha.
								Mean/rms				Mean/rms			
I	48/94	01/10/86-02/12/86	13.5	113.4	43.8	1.0	12	13.2 /6.7	130.8 / 30.3	38.5 /12.5	14.2 /19.0	13.4 / 7.1	114.2 / 31.8	38.8 /13.7	356.9 / 20.8
C	52/53	01/11/86-03/08/86	29.5	4.9	26.0	89.3	3	47.1 / 8.5	13.2 / 10.4	39.3 /10.9	81.3 / 6.1	37.6 / 2.4	25.2 / 3.7	32.7 / 9.0	95.1 /16.0
B	38/75	01/12/86-04/12/86	18.1	6.3	32.5	148.1	17	22.5 / 8.6	13.2 / 22.5	34.2 /14.5	164.7 / 25.1	19.8 / 7.8	18.7 /23.3	29.9 /15.2	172.3 / 30.6
	74/75		11.8	14.4	22.3	138.8									
F	70/96	01/10/86-03/19/86	5.2	7.9	39.8	20.9	17	9.8 /4.3	9.6 /26.1	38.4 /14.8	10.3 /22.7	8.8 / 4.2	13.0 / 28.7	36.1 / 8.9	13.3 /14.3
	95/96		8.3	354.6	25.8	16.1									
E	63/64	01/11/86-04/12/86	20.0	347.8	25.0	42.3	27	28.7 /10.7	26.4 /21.9	42.6 /14.4	71.2 /19.7	26.8 / 8.0	24.5 /17.3	40.0 / 7.7	68.6 /11.1
H4	20/60	06/22/83-07/02/83	21.1	99.1	64.4	347.4	7	15.3 / 8.3	105.6 / 33.0	63.2 /22.1	3.0 /20.5	12.1 /11.8	115.0 / 78.3	51.1 /13.0	359.4 / 14.8
E2	20/60	03/03/84-04/04/84	30.8	7.2	35.4	51.2	30	27.4 /11.8	23.4 /25.4	39.9 /16.5	69.3 /24.4	26.5 / 9.4	20.7 /20.8	38.2 /10.6	66.1 /16.1
	45/60		26.1	345.1	29.9	39.0									
H3	20/63	03/05/84-04/11/84	11.0	109.8	67.2	354.9	2	18.7 / 3.8	140.2 / 11.8	46.8 / .4	340.9 / .5	27.2 / 1.4	146.2 / 2.9	66.9 / 8.7	336.9 / 7.4
	45/63		7.0	90.7	59.0	349.1									
H5	90/92	03/05/84-03/26/84	5.4	92.8	28.8	347.2	28	9.2 / 6.6	127.0 / 46.3	41.7 /16.6	15.5 / 23.5	9.2 / 5.4	125.9 / 35.8	39.1 /15.0	14.6 / 22.7
MJ	60/75	02/24/86-04/23/86	22.8	130.3	67.5	312.9	4	31.2 /11.1	157.1 / 20.9	47.0 / 6.4	7.4 / 7.8	36.9 / 9.2	126.9 / 14.5	55.2 /10.6	338.1 / 11.1

trajectories are in good agreement with the moored M_2 currents, we have computed M_2 currents using all available trajectories shown in Fig. 1. To offset estimation errors caused by local topography and observation time, we average M_2 currents of truncated drifter data in 0.5 degrees by 0.5 degrees rectangular boxes and discard boxes where number of the truncated series are less than five. Fig. 11 shows a spatial distribution of box-averaged M_2 current ellipses. Ellipses marked by full and broken lines mean, respectively, clockwise and counterclockwise rotations. In general, shape of ellipses varies with latitude; circular in the southern YS and the boundary zone between the YS and the East China Sea, rectilinear at latitudes of 34° 30'-35° 30'N, and circular north of 35° 30'N. The rotation direction of ellipses changes its sign around 35° 30'N from the clockwise direction to the south to the counterclockwise one

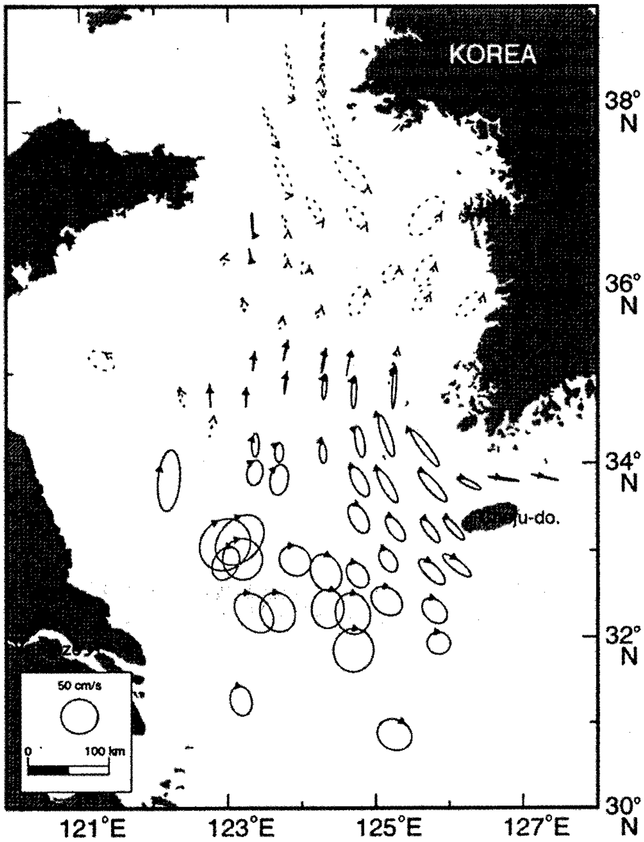

Fig. 11. Spatial distribution of 0.5 degrees-by-0.5 degrees box-averaged M_2 tidal current ellipses in the Yellow Sea, estimated from all available drifter trajectories. Ellipses marked by full and broken lines mean, respectively, clockwise and counterclockwise rotations.

to the north, with exceptions in coastal areas east and south of the Shandung peninsula where amphidromic points are located. M_2 current is strong off the Changjiang River estuary and in the Korean coastal area, while it is weak in the deep central area of the YS. The rotation direction based on the drifter experiment is in generally good agreement with that computed by tide models (e.g., Choi, 1980; Kang *et al.*, 1998). The clockwise rotation in a very limited area off the eastern tip of the Shandung peninsular is also remarked in a fine grid tide model (Kang *et al.*, 1998). A difference between the model results by Kang *et al.* (1998) and our computation is seen in the Cheju Strait. The model M_2 currents show change of rotation direction there; clockwise in the western entrance of the Cheju Strait but counterclockwise in the eastern Cheju Strait, while the box-averaged M_2 currents show only the clockwise rotation. When we look into individual M_2 currents prior to the box-averaging, the counterclockwise rotation is also seen from some trajectories. Both of the computed and model M_2 current ellipses in the Cheju Strait are almost rectilinear, although the rotation direction of rectilinear tidal ellipses is not so meaningful as that of elliptical or circular ellipses.

CONCLUSIONS

We have developed an effective method for estimating diurnal and semi-diurnal tidal currents from drifter trajectories. This estimation method can be applied to area where tidal current signals are significantly higher than background noise levels. However, prior to its application, it is necessary to check carefully sampling interval of position fixes, data truncation, and separation of low-frequency current signals for a better estimation. The method can compute major tidal currents with high accuracy, provided that the time span T of truncated serial data is properly chosen and the signal-to-noise level is low. For a better estimation, the time span T of boxcar window should be chosen according to the low-frequency currents; long in weak mean current area but short in strong mean current area. In order to decrease the signal-to-noise level in tidal frequency bands, we need to apply a proper method to eliminate the low-frequency signals. Low-frequency current signals in drifter trajectories can be separated by both filtering and fitting. Although the second-order polynomial fitting used in this study is a good method, it does not filter out effectively important low-frequency signals contained in the beginning and ending parts of truncated time series.

Application of the developed method to all available drifter trajectories in the YS has provided the spatial distribution of the most dominant M_2 tidal current in the YS, for the first time based on directly measured current data. The good agreement between M_2 currents computed from moored current data and drifter trajectories in the vicinity of the mooring points supports not only the validity of this method but also the reliability of the M_2 current chart in the YS. It is concluded that this method can effectively estimate major diurnal and semi-diurnal currents from drifter position data and moored current data, provided signal-to-noise levels in the corresponding frequency bands are sufficiently low and the data truncation is adequately chosen.

ACKNOWLEDGEMENTS

This study has been performed as part of two projects on the Yellow Sea Circulation and Material Flux and the Coastal Ocean Processes for Marine Pollution in the Yellow Sea, funded by the Korean Ministry of Science and Technology. The final version of the manuscript was prepared during the senior author's visit as visiting professor to Research Institute for Applied Physics, Kyushu University. The authors give their thank to Professor T. Yanagi for his reading a revised version of the manuscript.

REFERENCES

An, H.S., 1977. A numerical experiment of the M_2 tide in the Yellow Sea. *J. Oceanogr. Soc. Jap.*, **33**: 103 − 110.

Choi, B.H., 1980. A tidal model of the Yellow Sea and Eastern China Sea. KORDI Rep. 80 − 02, KORDI, Seoul, 72 pp. (in Korean).

Guo, X. and T. Yanagi, 1998. Three-dimensional structure of tidal current in the East China Sea and the Yellow Sea. *J. Oceanogr.*, **54**: 651 − 668.

Hsueh, Y., 1988 Recent Current Observations in the Eastern Yellow Sea. *J. Geophy. Res.*, **93**: 6875 − 6884.

Kang, S.K., S.R. Lee, and H.-J. Lie, 1998. Fine grid tidal modelling of the Yellow and East China Seas. *Cont. Shelf Res.*, **18**: 739 − 772.

Kang, S.K., S.R. Lee, and K.D. Yum, 1991. Tidal computation of the East China Sea, the Yellow Sea, and the East Sea. In: Oceanography of Asian Marginal Seas, Elsevier Oceanogr. Series, **54**: 25 − 48.

Lie, H.-J., 1998a. Ocean circulation in the western and middle part of East China Sea (First year). KORDI Rep. BSPE 97603-00-1042-1, 278 pp. (in Korean).

Lie, H.-J., 1998b. A study on water circulation and material flux in the Yellow Sea - Current measurements and circulation of the Yellow Sea. KORDI Rep. BSPN 97357-01-1102-1, 348 pp. (in Korean).

Lie, H.-J., 1999. On the Huanhai (Yellow) Sea circulation: a review by current measurements. *Acta Oceanol. Sinica*, **18**: 355 − 373.

Lie, H.-J., C.-H. Cho, J.-H. Lee, S. Lee, and Y. Tang, 2000. Seasonal variation of the Cheju Warm Current in the northern East China Sea. *J. Oceanogr.*, **56**, 197 − 216.

Munk, W.H. and C. Hasselman, 1964. Super resolution of tides. In: Studies in Oceanography, Univ. of Tokyo, 339 − 344.

Nishida, H. 1980. Improved tidal charts for the western part of the north Pacific Ocean. *Rep. Hydrogr. Res.*, No. 15.

Ogura, S., 1933. The tides in the sea adjacent to Japan. *Bull. Hydrogr. Depart.*, Imperial Japanese Navy, **7**: 1 − 189.

Sybrandy, A.L. and P. Niiler, 1991. The WOCE/TOGA SVP Lagrangian drifter construction manual. WOCE Rep. 63, Scripps Inst. of Oceanogr., Univ. of Calif., La Jolla, 58 pp.

WOCE, 1991. Report of the Third Meeting (SVP-3) with focus on the Pacific Sector of WOCE/TOGA Surface Velocity Programme Planning Committee. WOCE Rep. No. 65/91, 24 pp.

Zetler, B.D., M.D. Schuldt, R.W. Whipple and S.D. Hicks, 1965. Harmonic analysis of tides from data randomly spaced in time. *J. Geophy. Res.*, **70**: 2805 − 2811.

Manuscript received September, 13, 1999
Revision accepted January, 25, 2000
Editorial Handling: Ig-Chan Bang